Embrittling and strengthening effects of hydrogen, boron, and phosphorus on a $\Sigma 5$ nickel grain boundary

W. T. Geng and A. J. Freeman
Department of Physics and Astronomy, Northwestern University, Evanston, Illinois 60208

R. Wu
Department of Physics and Astronomy, California State University, Northridge, California 91330

C. B. Geller
Bettis Atomic Power Laboratory, West Mifflin, Pennsylvania 15122-0079

J. E. Raynolds
Lockheed Martin, Schenectady, New York 12301-1072

(Received 10 March 1999)

The embrittling and strengthening effects of hydrogen, boron, and phosphorus on a $\Sigma 5(210)$ [100] nickel grain boundary are investigated by means of the full-potential linearized augmented plane-wave method with the generalized-gradient approximation formula. Optimized geometries for both the free surface and grain-boundary systems are obtained by atomic-force calculations. The results obtained show that hydrogen and phosphorus are embrittlers and that boron acts as a cohesion enhancer. An analysis of the atomic, electronic, and magnetic structures indicates that atomic size and the bonding behavior of the impurity with the surrounding nickel atoms play important roles in determining its relative embrittling or cohesion enhancing behavior. [S0163-1829(99)02926-4]

I. INTRODUCTION

It is now well recognized that mechanical properties such as the brittleness of an engineered material can be significantly changed by small concentrations of impurities that segregate to the grain boundaries.[1] A thermodynamic theory developed by Rice and Wang[2] describes the mechanism of the metalloid-induced intergranular embrittlement through the competition between plastic crack blunting and brittle boundary separation. According to this theory, the potency of a segregation impurity in reducing the ''Griffith work'' of a brittle boundary separation is a linear function of the difference in binding energies for that impurity at the grain boundary and the free surface. That is, if the grain boundary is more energetically favored by an impurity than the free surface, its resistance to brittle intergranular fracture is enhanced by this impurity. With the aid of high performance supercomputers, it is now feasible to employ state-of-the-art first-principles local-density electronic structure approaches to determine the binding energy of an impurity at the grain boundary and at the free surface; and in turn, the embrittling and strengthening effects of this impurity on this grain boundary.[3,4]

Unlike Ni-based alloys such as Ni_3Al, which have been extensively investigated in recent years, the effects of impurities on the grain boundaries of pure Ni have not. Crampin *et al.*[5] studied the electronic structure and the effect of the S segregant on the cohesion properties of the Ni $\Sigma 5(210)$ grain boundary using the layer Korringa-Kohn-Rostoker method. In these early calculations, however, they could not include atomic relaxations and employed only four k points in the two-dimensional Brillouin zone for the determination of the electronic structure. For S, the substitutional site, rather than the interstitial one, was chosen in order to avoid large strain, and so S was an addition rather than an impurity. Recently, Wang and Wang[6] studied the effects of boron and sulphur on the electronic structure of the Ni $\Sigma 11(113)$ grain boundary by means of a discrete variational method applied to molecular clusters. In the present work, we employed the full-potential linearized augmented plane-wave (FLAPW) method[7] to investigate the effects of H, B, and P impurities on the $\Sigma 5(210)$ grain boundary of nickel and the nickel (210) free surface. Fully relaxed atomic structures of the impurites, the surrounding Ni atoms in the grain boundary, and the clean surface environments were obtained by minimizing the total energies as directed by the calculated atomic forces. The calculated atomic, electronic, and magnetic features were then used to analyze the physics behind the embrittling and strengthening behavior of these impurities. The rest of the paper is organized as follows. In Sec. II, we present the model and computational details. Results of the geometric relaxation and magnetic interactions are discussed in Sec. III. In Sec. IV, we interpret the chemical interactions. The mechanism for the cohesive properties of H, B, and P at the Ni $\Sigma 5(210)$ grain boundary is discussed in Sec. V, and in Sec. VI, we give a short summary.

II. MODEL AND COMPUTATION

As sketched in Fig. 1, both the $X(X=\mathrm{H, B,}$ and $\mathrm{P})$/Ni(210) free surface (panel a) and the X/Ni $\Sigma 5(210)$ grain boundary (panel b) were simulated by a slab model,[8] which

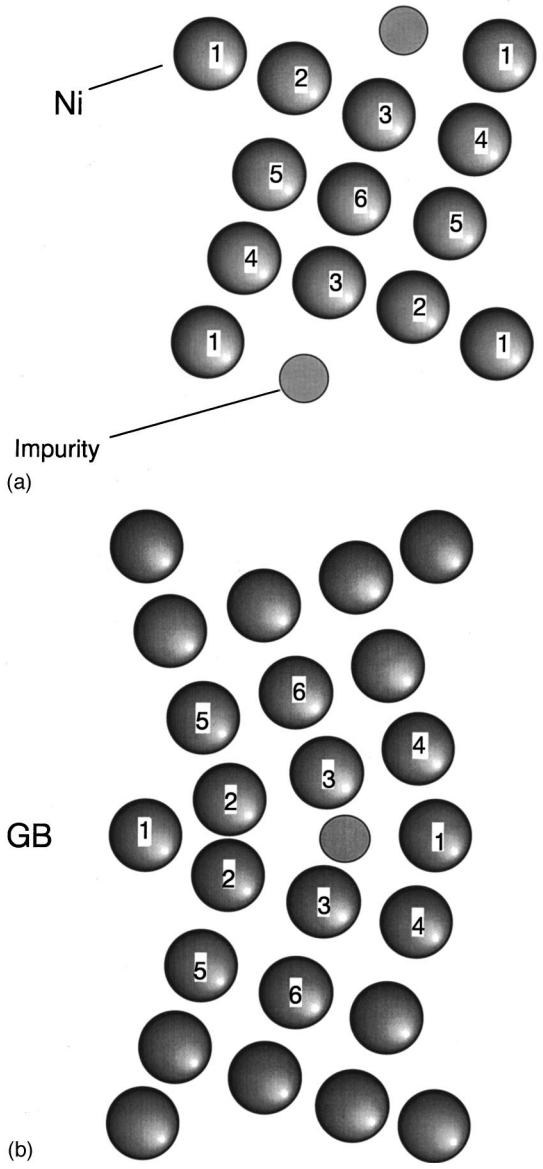

FIG. 1. Model and notation for the structure of the Ni and impurity at (a) the Ni (210) free surface and (b) the $\Sigma 5$ (210) [100] grain boundary.

minimizes the impurity-impurity interactions inherent in the use of superlattice cells. For the X/Ni(210) free-surface (FS) systems, the Ni(210) substrate was simulated by an 11-layer slab, and the X adatoms were placed pseudomorphically on the next Ni sites on both sides of this slab. For the grain-boundary (GB) system, a 21-layer slab was adopted to simulate the clean Ni $\Sigma 5(210)$ GB, and the X adatom was placed at the hollow site in the GB core. With nine layers of Ni atoms in-between, the remaining FS-FS and FS-GB interactions were expected to be sufficiently reduced. The two-dimensional lattice constant was chosen to be that of the bulk value for fcc Ni, 6.64 a.u., that was also reproduced in our generalized-gradient approximation (GGA) calculation. The (210) interlayer distance for the ideal system (GGA bulk) is therefore 1.48 a.u.

In the FLAPW method, no shape approximations are made to the charge densities, potentials, and matrix elements. For both the nickel and impurity atoms, the core states are treated fully relativistically and the valence states are treated semirelativistically (i.e., without spin-orbit coupling). The GGA formulas for the exchange-correlation potential are from Perdew *et al.*[9] An energy cutoff of 13 Ry was employed for the augmented plane-wave basis to describe the wave functions in the interstitial region, and a 140 Ry cutoff was used for the star functions depicting the charge density and potential. Muffin-tin radii for Ni, H, B, and P atoms were chosen as 2.0, 1.0, 1.3, and 1.8 a.u., respectively. Within the muffin-tin spheres, lattice harmonics with angular momentum l up to 8 were adopted.

Convergence was assumed when the average root-mean-square differences between the input and output charge and spin densities are less than $2\times10^{-4}e/(\text{a.u.})^3$. The equilibrium atomic positions in the vertical direction of both the X/Ni FS and X/Ni GB systems, and their corresponding clean reference systems, were determined according to the calculated atomic forces. The structure within the lateral (210) plane was kept unchanged to maintain the in-plane symmetry. In order to simulate the bulklike environment for the GB case, we fixed the positions of the three outermost Ni layers and adjusted the others around the GB core. Equilibrium relaxed structures were assumed when the atomic forces on each atom (except for those on the outermost three layers in the GB case) became less than 0.002 Ry/a.u. To speed up the calculations, the step-forward approach[10] was used.

The binding-energy difference of an impurity in the FS and GB environments is very small. Hence, to obtain a reliable binding energy difference, the FS and GB systems must be treated on an equal footing and the atomic structures of the FS and GB should also be optimized for the cases with and without impurity atoms. Bearing this in mind, we used the same set of numerical parameters in the FLAPW calculations for both the GB and FS; and the calculated atomic, electronic, and magnetic structures are given for the fully relaxed systems.

However, in a numerical implementation of any algorithm, one always has to replace infinite series and continuous integrations by finite sums, which leads to numerical errors. A very important aspect of the FLAPW method for solving the Kohn-Sham equations is the absence of uncontrolled numerical parameters. This means that we are always able to calculate the accuracy of our results, and that we know how to make improvements when the errors are too large.

To predict whether an impurity is an embrittler or a cohesion enhancer to a hosting grain boundary, the total energy of five systems must be given with high precision. These five systems, as mentioned above, are (1) the fully relaxed X present GB, (2) the fully relaxed clean GB, (3) the fully relaxed X present FS, (4) the fully relaxed clean FS, and (5) a monolayer of X at the appropriate lattice spacing. The numerical parameters inherent to the FLAPW method that influence the total energy have been discussed elsewhere in detail.[11,12] Aided by this experience, we can easily control all of these parameters, ensuring that the numerical error in the GB total energy is less than 0.02 eV. Since total-energy errors can be largely cancelled for two closely related systems, it is expected that the error in binding energy is much smaller than 0.02 eV.

TABLE I. Calculated interlayer distances (a.u.) of the X/Ni FS systems (starting from the FS).

Layer	Clean FS	H/Ni FS	B/Ni FS	P/Ni FS
d_{I1}		−0.03	0.02	0.64
d_{12}	1.32	1.28	1.34	1.64
d_{23}	1.47	1.59	1.90	1.67
d_{34}	1.58	1.64	1.40	1.47
d_{45}	1.47	1.53	1.52	1.50
d_{56}	1.51	1.51	1.49	1.49

As mentioned above, a force of less than 0.002 Ry/a.u. is viewed as zero. This results in an error to the atomic position of about 0.01–0.02 a.u. Therefore, for the reported calculations, the accuracy of the atomic structures is 0.02 a.u. Such errors in atomic structure result in a total energy error of about 0.01 eV. Thus, taking all of the above into account, the numerical accuracy of the impurity-GB binding energy is within 0.05 eV.

III. ATOMIC STRUCTURES AND MAGNETIC INTERACTIONS

The calculated interlayer distances for each system are listed in Table I (FS) and Table II (GB). For the clean Ni(210) surface, our total-energy–atomic-force calculations found that the surface layer Ni(1) undergoes a downward relaxation by 0.07 a.u., while both the second and the third layer go up by 0.09 a.u. All the other inner layers appear to not move much during the formation of a free (210) surface. The displacements of the top three layers result in a surface smoothing and make the interlayer distances at the Ni (210) surface show an oscillatory pattern, as known for other surfaces.[13]

A similar oscillation also occurs in the vicinity of the Ni GB. The interfacial Ni(2) layer is pushed away by as much as 0.55 a.u., due to the strong repulsion across the GB. The displacement of Ni(3) in the GB, however, is only 0.03 a.u. Large displacements were also found for Ni(4) (by 0.15 a.u.) and Ni(5) (by 0.23 a.u.) atoms. Overall, there is a long-range oscillatory pattern for the Ni interplanar distances away from the GB. Such an oscillation can be mainly due to steric effects, i.e., each atom tries to keep all its neighbors in bulk-environment positions. The small relaxations beyond the seventh Ni layer indicate that the GB effects are limited to a range of about six atomic layers on each side of the GB.

TABLE II. Calculated interlayer distances (a.u.) of the X/Ni GB systems (starting from the GB).

Layer	Clean GB	H/Ni GB	B/Ni GB	P/Ni GB
d_{12}	2.03	2.04	2.07	2.20
d_{23}	0.97	0.96	1.28	1.40
d_{34}	1.60	1.60	1.35	1.26
d_{45}	1.55	1.55	1.54	1.54
d_{56}	1.29	1.29	1.37	1.32
d_{67}	1.53	1.51	1.39	1.36
d_{78}	1.51	1.53	1.53	1.52

Therefore, the 21-layer slab used here is sufficient to capture the properties of the Ni(210) GB.

Unlike P, the H and B atoms are actually diffused below the surface Ni layer, due to their small sizes. However, the atomic structure of the host Ni(210) surface differs quite remarkably for the H and B cases. The Ni-Ni interlayer distances with B show a much stronger oscillation, due to the drastic downward relaxation of Ni(3). Such a long-range change is also found in the P/Ni FS system, indicating the stronger effects of B and P on Ni-Ni bond lengths than does H.

As required by the z-reflection symmetry of the GB, the impurity atom stays in the same vertical position as Ni(1). Compared with the relaxed clean GB, the presence of H or B only slightly changes the position of Ni(2) (0.01 a.u. for H and 0.04 a.u. for B); but the P atom pushes these two Ni(2) atoms further apart (0.17 a.u.). This can be understood from the fact that the atomic size of P is much larger than those of H and B. Unlike H (0.01 a.u.), B and P significantly change the position of Ni(3) by 0.35 and 0.60 a.u., respectively. Compared with the free surface cases, the bond lengths of both H-Ni(3) and B-Ni(3) are expanded in the GB environment. By contrast, the P-Ni(3) bond is apparently compressed in the GB. Quantitatively, the H-Ni(3) bond length increases from 3.20 (FS) to 3.35 a.u. (GB), while the B-Ni(3) bond length increases from 3.58 (FS) to 3.66 a.u. (GB). On the contrary, the P-Ni bond length decreases from 4.22 (FS) to 3.89 a.u. (GB).

To learn more about the effects of an impurity atom on the GB, it is helpful to compare the GB relaxation with the FS relaxation induced by this impurity. Among the three impurities, B shows the strongest influence on the Ni atomic structure in the FS environment. The atomic size of the impurity appears not to be very important in the FS case, since the impurity has freedom to adjust into the vacuum. Comparatively, P affects the Ni atomic structure mostly in the GB surroundings. This can be understood from the fact that P is much larger in size than B; and, hence it cannot be well hosted in the GB without pushing the Ni atoms [especially Ni(3)] apart. Due to its large atomic size, the segregation of P at the GB inevitably results in a significant cost of Ni-Ni bonding energy. On the other hand, the compressed P-Ni bond length also reduces the P-Ni bonding energy. As discussed in the following sections, both the contraction of the P-Ni bond and the expansion of the GB core play important roles in the embrittling effects of P on the Ni $\Sigma 5(210)$ GB.

Spin-density difference contours for the X/Ni FS and GB systems are shown in Figs. 2–4, respectively. The calculated magnetic moments of the Ni and impurity atoms in different environments are listed in Table III (FS) and Table IV (GB).

The magnetic interaction between the metalloid and the surrounding Ni atoms varies with the environment, as can be seen from the shape of the spin-transfer contours in Figs. 2–4. All of these impurities have apparently detrimental effects on the Ni magnetization at the FS or GB, mainly due to the hybridization and related effects between X and the surrounding Ni atoms. The strength of the detrimental effect of each impurity is roughly in accordance with its influence on the atomic structure. As mentioned above, H has the weakest influence on the atomic structure in either the FS or the GB cases. Also evident here, is that H has the smallest influence

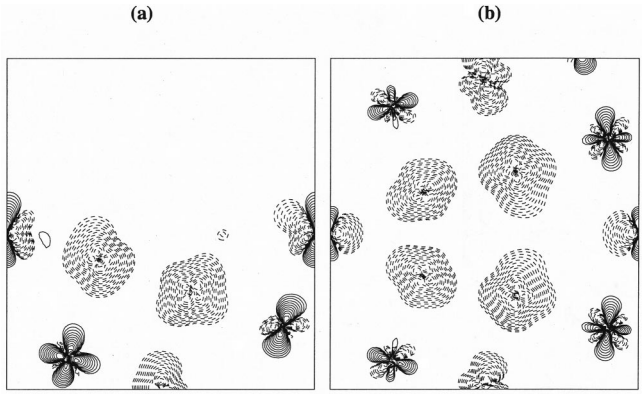

FIG. 2. The calculated spin-density difference for (a) the H/Ni FS and (b) the H/Ni GB. Contours start from $7\times10^{-4}e$/a.u.^{3} and increase successively by a factor of $\sqrt{2}$. Dashed and solid lines denote spin depletion and accumulation, respectively.

on the magnetization of the Ni atoms. The magnetic moment of Ni(1) in the FS, for example, experiences a reduction of $0.11\mu_B$ in the presence of H; while in the cases of B and P, it is reduced by as much as 0.56 and $0.79\mu_B$, respectively. In fact, P reduces the magnetization almost completely for the Ni(1) and Ni(2) atoms, while significantly reducing the Ni(3) magnetization in both the FS and GB cases. Again for Ni(1), the reduction of its magnetic moment in the GB is $0.07\mu_B$ (H), $0.52\mu_B$ (B), and $0.62\mu_B$ (P), respectively. The impurity effects on the Ni magnetization, however, appear to be limited to the first rank of neighbors. Starting from Ni(4), the Ni magnetic moments gradually restore the bulk value, 0.60–$0.61\mu_B$. In both the FS and the GB cases, the induced magnetic moment for X is within $0.01\mu_B$: less than $-0.01\mu_B$ for the H, and $0.01\mu_B$ for both B and P.

IV. CHEMICAL INTERACTION

The charge density plays the key role in an analysis of interatomic bonding mechanisms. The formation, dissolution, strengthening, and weakening of chemical bonds are always characterized by charge accumulation and depletion. In Figs. 5–7, charge-density differences, obtained for each system by subtracting the superimposed charge density of a free X monolayer and the clean Ni reference slab from the charge density of the corresponding X/Ni system, are presented for the X/Ni FS (panel a) and X/Ni GB (panel b), respectively.

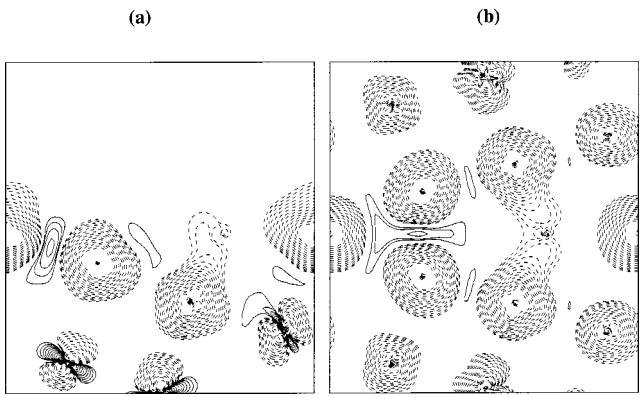

FIG. 3. The calculated spin-density difference for (a) the B/Ni FS and (b) the B/Ni GB. Contours start from $7\times10^{-4}e$/a.u.^{3} and increase successively by a factor of $\sqrt{2}$. Dashed and solid lines denote spin depletion and accumulation, respectively.

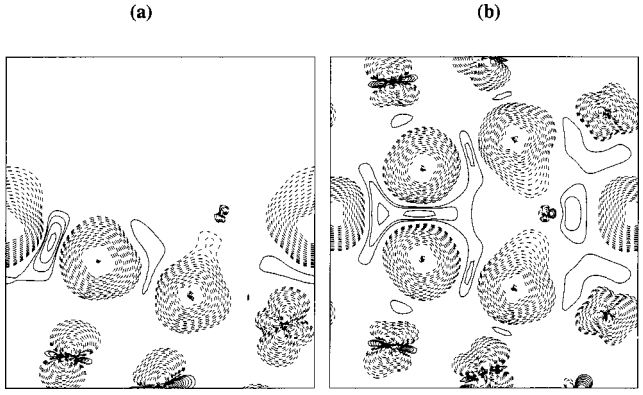

FIG. 4. The calculated spin-density difference for (a) the P/Ni FS and (b) the P/Ni GB. Contours start from $7\times10^{-4}e$/a.u.^{3} and increase successively by a factor of $\sqrt{2}$. Dashed and solid lines denote spin depletion and accumulation, respectively.

Comparing the charge-density difference between different X/Ni systems, reveals that for all of them the interaction of the X and Ni atoms is restricted to a local region near the impurity. Although the geometrical relaxation, as discussed above, extends beyond this area. For each X, significant electron accumulation is found between the X and Ni(3) atoms in both FS and GB cases, pointing to prominent chemical interactions between them. A more detailed comparison shows that except for its nearest-neighbor Ni(3), the net effect of H is mainly to attract electrons from the nearby region, and, hence, to promote poor local cohesion. By contrast, B and P significantly change the charge distribution inside the muffin-tins of Ni(1) and Ni(2), indicating a stronger chemical perturbation.

As for bonding characteristics of X-Ni(3), each X shows different features. For H-Ni(3), only charge accumulation is found on the H side in the region between H and Ni(3), indicating an apparent ionic character. This can be explained by the electronegativity difference between H (2.20) and Ni (1.91). By contrast, the charge depletion is found in the inner region of both B and P, pointing to the covalent feature of the B-Ni(3) and P-Ni(3) chemical interaction. However, unlike B, the P turns out to be an electron donor in both the FS and GB environment, as seen in Fig. 7. This apparent reverse charge transfer contradicts the trend estimated from the elec-

TABLE III. Calculated magnetic moments (μ_B) of Ni and the impurity atoms for the X/Ni FS systems (starting from surface.)

Atom	Clean FS	H/Ni FS	B/Ni FS	P/Ni FS
Impurity		0.00	−0.01	−0.01
Ni(1)	0.79	0.68	0.23	0.00
Ni(2)	0.71	0.52	0.09	0.01
Ni(3)	0.66	0.45	0.30	0.24
Ni(4)	0.63	0.63	0.59	0.51
Ni(5)	0.61	0.68	0.63	0.56
Ni(6)	0.60	0.60	0.61	0.60

TABLE IV. Calculated magnetic moments (μ_B) of Ni and the impurity atoms for the X/Ni GB systems (starting from GB).

Atom	Clean GB	H/Ni GB	B/Ni GB	P/Ni GB
Impurity		0.00	−0.01	−0.01
Ni(1)	0.67	0.60	0.15	0.05
Ni(2)	0.68	0.59	0.25	0.12
Ni(3)	0.67	0.51	0.27	0.25
Ni(4)	0.65	0.64	0.54	0.55
Ni(5)	0.63	0.63	0.56	0.58
Ni(6)	0.61	0.64	0.61	0.60

tronegativities (2.19 for P and 1.91 for Ni). Such behavior can be understood from the large spatial extent of the P $3p$ wave function and, thus, the *embedding* character of the P-Ni bonding. Also worth noting is that the B-Ni(1) bond shows a similar character to the P-Ni(1) bond. Due to the smaller spatial extent of the B $2p$ (compared with the P $3p$) wave function, however, the *embedding* feature is not as prominent.

Quantitatively, the strength of the chemical interaction between an impurity and FS or GB is represented by its binding energy which, in the slab model, is defined as

$$\Delta E_s = E(FS) + E(X) - E(X/FS)$$

and

$$\Delta E_b = E(GB) + E(X) - E(X/GB),$$

where $E(X)$, $E(FS)$, $E(X/FS)$, $E(GB)$, and $E(X/GB)$ represent total energies of the X monolayer, clean FS, X adsorbed FS, clean GB, and X segregated GB slabs, respectively. The calculated binding energies of H, B, and P with the Ni (210) FS and Ni $\Sigma 5(210)$ GB are listed in Table V. For both H and P, the binding energies decrease from the FS to the GB, while for B the larger binding energy is in GB. Different from the FS case, where P has the largest binding energy, B is more favored by the GB system than P and H.

To gain more physical insight, it is helpful to separate the binding energies into two parts. One is from the direct interaction between impurity and host atoms, defined as the work needed to remove the impurity while not permitting the Ni atoms to relax; the other is the total-energy change of the host-host interaction induced by the impurity, defined as the energy release (with reverse sign) during the course of Ni relaxation after the impurity is removed. The former, also called the *chemical contribution*, almost always enhances the impurity-host binding; while the latter, also called the *mechanical contribution* and represented by the relaxation energy change, always weakens the total binding energy. The binding energy, and also the optimized atomic structure, is then determined by the combination of these two contributions. To demonstrate numerically, we need to calculate, besides the five systems mentioned in Sec. II, another two reference systems—X removed but Ni atoms unrelaxed, one for the FS and the other for the GB. The calculated chemical and mechanical contributions of each impurity in the GB and FS cases are listed in Table V.

To answer the question why H experiences a chemical energy (*chemical contribution* to the binding energy) reduction from the FS to the GB, we analyzed the environmental changes. The most important changes included the expansion of the H-Ni(3) bond length and the additional Ni(3) neighbor

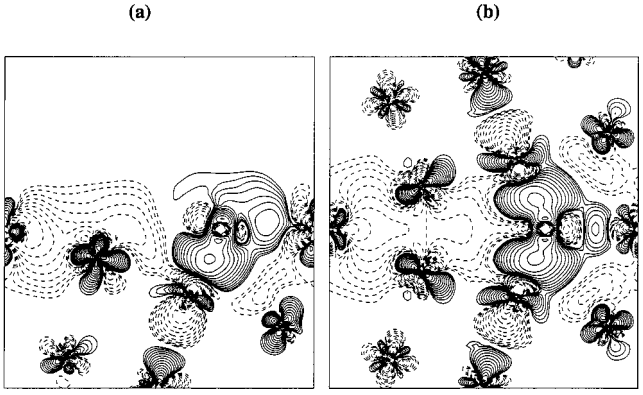

FIG. 6. The calculated valence charge-density difference for (a) the B/Ni FS and (b) the B/Ni GB. Contours start from 7 $\times 10^{-4} e$/a.u.^{3} and increase successively by a factor of $\sqrt{2}$. Dashed and solid lines denote charge depletion and accumulation, respectively.

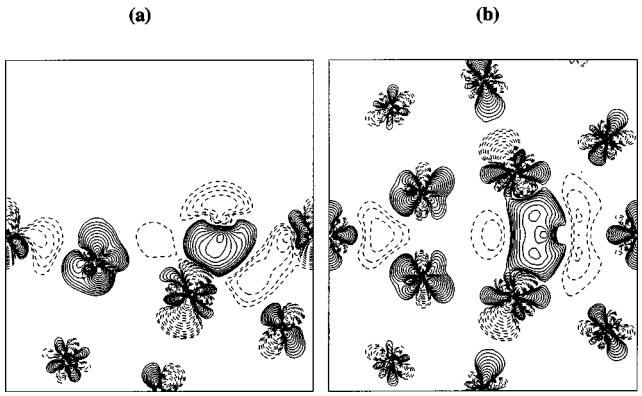

FIG. 5. The calculated valence charge-density difference for (a) the H/Ni FS and (b) the H/Ni GB. Contours start from 7 $\times 10^{-4} e$/a.u.^{3} and increase successively by a factor of $\sqrt{2}$. Dashed and solid lines denote charge depletion and accumulation, respectively.

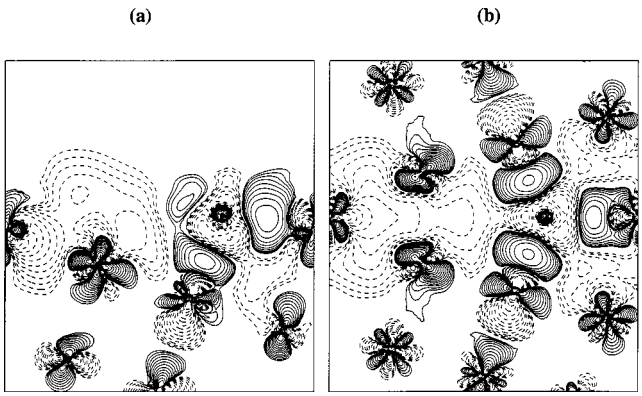

FIG. 7. The calculated valence charge-density difference for (a) the P/Ni FS and (b) the P/Ni GB. Contours start from 7 $\times 10^{-4} e$/a.u.^{3} and increase successively by a factor of $\sqrt{2}$. Dashed and solid lines denote charge depletion and accumulation, respectively.

TABLE V. Binding energies (eV) and the mechanical and chemical contributions of X/Ni FS and X/Ni GB systems.

	H/Ni(FS)	B/Ni(FS)	P/Ni(FS)	H/Ni(GB)	B/Ni(GB)	P/Ni(GB)
Binding energy	3.26	6.34	6.36	2.99	6.83	5.66
Mechanical	−0.14	−0.27	−0.30	−0.01	−0.16	−0.65
Chemical	3.40	6.61	6.66	3.00	6.99	6.31

in the GB. From the charge-density differences for the FS and the GB given in Fig. 5, the charge gain for H is about the same in the FS and GB environments, implying that the bonding capability of H has already been saturated in the FS environment. However, this observation cannot yield even a qualitative explanation of the H binding energy difference between the FS and GB environment, because it is not easy to compare the chemical energy of one strong bond (the FS case) and two weak bonds (the GB case) just from plots.

To separate the issues from the expanded bond length and the additional bond with the other Ni(3) atom, we employed an artificial model FS atomic structure. This structure was obtained from the fully relaxed H/Ni FS atomic structure by raising the H by 0.15 a.u., raising the Ni(1) by 0.12 a.u., and keeping all the other Ni atoms fixed. The H-Ni(3) and H-Ni(1) distances in this artificial model structure are exactly the same as those in the GB case. Our calculations show that the chemical energy for this artificial model FS atomic structure is 3.29, or 0.11 eV smaller than that in the fully relaxed FS case. This means that the expansion of the H-Ni(3) bond has a detrimental effect on the chemical energy of H by 0.11 eV. In going from this artificial model FS atomic structure to the GB, the chemical energy of H decreases further by 0.29 eV. Since the main change of environment felt by H is the addition of another Ni(3), this 0.29 eV decrease should be mainly due to the additional Ni(3). Therefore, the enlarged number of bonding Ni atoms is the main cause that makes H have a smaller chemical energy in the GB systems.

As stated in Sec. III, the bond length of B-Ni(3), similar to H-Ni(3), also experiences an expansion from FS to GB environment. However, since the expansion of the B-Ni(3) bond length from the FS to the GB environment is only 0.08 a.u., the strength of the B-Ni(3) bond is not expected to change much. Our artificial model FS atomic-structure calculation shows that the B-Ni(3) bond expansion has a detrimental effect of only 0.04 eV. Therefore, the chemical energy increase should be mainly due to the additional B-Ni(3) bond. It is interesting to note that the increase of the number of bonds has a quite different effect on H and B. From the FS to the GB, the charge accumulation in the region between B and Ni(1) is apparently decreased, pointing out that the B-Ni(1) bond is significantly weakened. However, since the strong dangling bond in the FS surroundings is saturated in the GB case, the GB environment is still more energetically favored by the B than the FS.

Different from H and B, P experiences a more conspicuous change of its bond length with Ni(3). The P-Ni(3) bond has a length of 4.22 a.u. in the FS case, but only 3.89 a.u. in the GB. This contraction has a pronounced detrimental effect on the P-Ni(3) bond, which can be inferred from the weakened (compared with the FS case) charge accumulation in the region between P and Ni(3). Our artificial model FS atomic structure calculations also show that the P-Ni(3) bond contraction has a strong detrimental effect of 0.46 eV. From the artificial model FS structure to the GB, the chemical energy of P increases from 6.20 eV to 6.31 eV, mainly due to the additional P-Ni(3) bond. Comparable to the B-Ni(1) bond, the P-Ni(1) chemical interaction is also diminished in the GB environment. The additional P-Ni(3) bond proves unable to compensate for the energy loss. This is very interesting since the P-Ni binding energy in the FS is larger than in the GB, if the same bond length is adopted. This means that the difference in P-Ni binding energies from FS to GB is mainly due to the change in atomic structures.

V. EMBRITTLING AND STRENGTHENING BEHAVIOR AND DISCUSSION

The embrittling and strengthening behavior of H, B, and P in the nickel $\Sigma 5$ (210) grain boundary was then determined according to the Rice-Wang model[2] through the value and sign of the strengthening energy ΔE_B, which is defined as

$$\Delta E_B \equiv \Delta E_b - \Delta E_s ,$$

where ΔE_b and ΔE_s are the binding energies of the impurity at the GB and FS, respectively. The calculated ΔE_B of H, B, and P at the Ni $\Sigma 5$ (210) GB are listed in Table VI.

Since H and P have negative ΔE_B values, they are embrittlers. For B, ΔE_B is positive, and therefore B acts as a cohesion enhancer for the nickel $\Sigma 5(210)$ grain boundary. This is the first quantitative theoretical determination made on this system.

Now comes the long-standing question: what is the key factor that determines the behavior of an impurity on the cohesive properties of a grain boundary? Atomic size, number of valence electrons, or strength of hybridization? As mentioned above, the behavior of an impurity is determined by the difference of binding energies related to the impurity-host bond and the impurity-induced changes in host-host interaction in the FS and GB systems. Obviously, stronger impurity-host interactions in the GB are more likely to make the impurity a cohesion enhancer. Equally important is that the impurity-induced change in the host-host interaction in the GB case should be weaker than that in the FS environment. Combining the results of the present investigation with previous calculations on various other GB systems,[14–16] we conclude that the behavior of an impurity on the cohesive

TABLE VI. Strengthening energy, ΔE_B, of H, B, and P at the Ni$\Sigma 5(210)$ GB.

	H/Ni(GB)	B/Ni(GB)	P/Ni(GB)
ΔE_B	−0.27	0.49	−0.70

properties of a grain boundary is determined by the competition between the above factors. To be an enhancer, the atomic size of the impurity should neither be too small nor too large; but it should fit well into the GB. Otherwise, the *X*-host bond would be either too compressed or too expanded, which would inevitably result in significantly weakened (compared with the FS case) *X*-host interactions.

For the nickel $\Sigma 5(210)$ GB, the hydrogen is too small; thus the expansion of the H-Ni bond attenuates the chemical interaction between the H and host Ni atoms. On the other hand, the additional H-Ni(3) bond in the GB system further weakens the H-Ni interaction. As for boron, its size mismatch is smaller than hydrogen and the resulting energy gained by the additional B-Ni(3) bond overcompensates the energy disadvantage. Similarly, beryllium and carbon can also be anticipated to be cohesion enhancers. Since P is much larger than H and B, the energy disadvantage caused by size mismatch is also much larger and cannot be compensated by the increased number of bonding Ni atoms. Therefore, we also expect that aluminum, silicon, and sulphur, which have similar atomic size and bonding as phosphorus, would be embrittlers.

VI. SUMMARY

We employed the full-potential linearized augmented plane wave method with the generalized-gradient approximation formula to investigate the embrittling and strengthening effects of hydrogen, boron, and phosphorus on a $\Sigma 5(210)$ [100] nickel grain boundary. The atomic-force approach was used to determine the optimized geometries. Our numerical results show that hydrogen and phosphorus are embrittlers and that boron is a cohesion enhancer. By separating the effects of the changes of the *X*-Ni ($X=$H, B, and P) bond length and the *X*-Ni bond number, we have shown that the atomic size of the segregation atom and the *X*-Ni bonding characters play important roles in determining the relative embrittling or cohesion enhancing behavior of this metalloid impurity. Both the H and B have a small atomic size, but the ionic character of the H-Ni bond makes H an embrittler, while the more covalent B-Ni bond builds B as a grain-boundary cohesion enhancer. Although the P-Ni interaction is also strong and covalent like, the large atomic size causes P to be an embrittler.

[1] S. F. Pugh, *An Introduction to the Grain Boundary Fracture in Metals* (The Institute of Metals, London, 1991).

[2] J. R. Rice and J. S. Wang, Mater. Sci. Eng., A **107**, 23 (1989).

[3] J. R. Smith, T. Hong, and D. J. Srolovitz, Phys. Rev. Lett. **72**, 4021 (1994).

[4] J. E. Raynolds, J. R. Smith, E. R. Roddick, and D. J. Srolovitz, Phys. Rev. B **53**, 13 883 (1996).

[5] S. Crampin, D. D. Vvedensky, J. M. MacLaren, and M. E. Eberhart, Phys. Rev. B **40**, 3413 (1989).

[6] L. G. Wang and C. Y. Wang, Comput. Mater. Sci. **11**, 261 (1998).

[7] E. Wimmer, H. Krakauer, M. Weinert, and A. J. Freeman, Phys. Rev. B **24**, 864 (1981), and references therein.

[8] R. Wu, A. J. Freeman, and G. B. Olson, J. Mater. Res. **7**, 2403 (1992); G. L. Krasko and G. B. Olson, Solid State Commun. **76**, 247 (1990).

[9] J. P. Perdew, K. Burke, and M. Ernzerhof, Phys. Rev. Lett. **77**, 3865 (1996).

[10] R. Wu and A. J. Freeman, Comput. Phys. Commun. **76**, 58 (1993).

[11] H. J. F. Jansen and A. J. Freeman, Phys. Rev. B **30**, 561 (1984).

[12] W. T. Geng, Ph.D. thesis, Institute of Physics, Chinese Academy of Sciences, 1998.

[13] S. P. Chen, A. F. Voter, and D. J. Srolovitz, Phys. Rev. Lett. **57**, 1308 (1986).

[14] R. Wu, A. J. Freeman, and G. B. Olson, Phys. Rev. B **53**, 7504 (1996).

[15] L. Zhong, A. J. Freeman, R. Wu, and G. B. Olson (unpublished).

[16] L. Zhong, R. Wu, A. J. Freeman, and G. B. Olson, Phys. Rev. B **55**, 11 133 (1997).